Journal of the Chinese Society of Mechanical Engineers, Vol.47, No.2, pp 185~194 (2026)

Numerical Investigation On The Early Onset Of Natural Convection In A Cavity At Low Rayleigh Numbers

Messaouda BOULMAALI* and Abdelkader KORICHI**

Keywords：Natural convection in a cavity, low Rayleigh numbers, onset of convection, early stages.

ABSTRACT

This study employs computational methods to investigate the early onset of natural convection in a square cavity, focusing on the dynamics at low Rayleigh numbers using the open-source OpenFOAM software. Through detailed analysis of streamlines and Nusselt numbers, the research identifies a gradual initiation of flow, characterised by evolving patterns and complex dynamics. The study examines the influence of the Rayleigh number (Ra) on flow behaviour, revealing that the time required for perturbation decreases as Ra increases. The steady-state flow is obtained at approximately nondimensional time $\tau = 100$. This value is reduced to 18 for Ra = 1000. At very low Rayleigh number (Ra<250), convection is negligible ($\overline{Nu} \cong 1$)). As Ra increases, the convection begins to play a role and becomes noticeable for Ra>800 ($\overline{Nu} > 1$), reaching a value $\overline{Nu} = 1.124$ at Ra=1000. These findings offer valuable insights with practical applications in thermal management and fluid dynamics.

INTRODUCTION

The natural convection heat transfer phenomenon occurs in a wide array of engineering and natural systems, providing significant benefits, though it may also pose challenges in certain scenarios. It is widely applied in solar energy systems (Khan et al., 2020; Akbarzadeh et al. 2020; Xu et al., 2019; Tanny, and Tsinober, 1998; Serrano-Arellano et al. 2013) where efficient thermal energy exchange is critical for harnessing renewable energy.

Paper Received October 2025. Revised January 2026. Accepted February, 2026. Author for Correspondence: A. Korichi.

* *Graduate Student, Faculty of Technology, Laboratory of Mechanics, Physics and Mathematical Modelling (LMP2M), University of Medea 26000, Algeria.*

** *Professor, Faculty of Technology, Laboratory of Mechanics, Physics and Mathematical Modelling (LMP2M), University of Medea 26000, Algeria*

for electronic cooling circuits; ensuring electronic components operate within their optimal temperature ranges to improve performance and longevity. In comfort and climate control, natural convection is utilized in air conditioning systems, enhancing energy efficiency through improved air circulation. Furthermore, it supports the design of sustainable buildings by enabling natural ventilation strategies that enhance airflow and reduce energy consumption.

The versatility and eco-friendliness of natural convection-based systems make them indispensable in modern engineering. By leveraging heat transfer principles through fluid motion, these systems provide energy-efficient solutions across diverse industries, advancing sustainability and environmental friendliness. Extensive research focuses on thermal phenomena in enclosed cavities, aiming to achieve precise control over heat transfer. In various applications, researchers pursue two key objectives: optimizing heat exchange (Liu et al., 2019; Alam and Kim, 2018) and improving insulation properties (Batchelor, 1954; Sharma and Debbarma, 2022).

In the quest to enhance heat exchange, researchers investigate the intricate dynamics of closed cavities. Their efforts focus on optimizing heat transfer mechanisms, often leveraging principles of natural convection, radiation, and conduction. This pursuit is particularly relevant in fields such as engineering, where efficient heat dissipation is critical. For instance, in the design of advanced heat exchangers, closed cavities act as key components for increasing heat transfer rates, thereby enhancing the performance of thermal systems.

Conversely, in some cases, the primary goal is to enhance insulation capabilities. In these cases, researchers develop strategies to reduce heat transfer within closed cavities, creating a thermal barrier. Such efforts are invaluable in fields like building construction, where minimizing heat loss or gain is critical for energy efficiency. By analysing materials and cavity configurations, researchers design innovative insulation solutions with high thermal resistance, contributing to

sustainable building practices.

In summary, the exploration of thermal phenomena within enclosed cavities is a multidisciplinary pursuit, with applications spanning climate control, sustainable energy, and other fields. Manipulating heat transfer within these confined spaces enables innovation, energy conservation, and scientific advancement.

When analysing free convection flows in enclosed cavities, three factors are critical: the geometry of the cavity, the thermophysical properties of the fluid, and the temperature difference (Bejan, 1993). Numerous studies have explored natural convection heat transfer in enclosures (Ostrach, 1988; Bejan, 2013), where temperature gradients across the cavity drive fluid motion. The analysis of stability in confined fluids has significant practical implications, particularly in applications requiring precise control of heat transfer rates (Janssen and Henkes, 1995). Controlled flow can enhance or diminish heat transfer rates, depending on the application. Janssen and Henkes (1995) focus on two objectives: determining the dependence of the laminar-turbulent transition on the Prandtl number and analysing the physical mechanisms underlying the observed bifurcations. Their findings show that, in square cavities, the transition occurs in periodic and quasi-periodic flow regimes for Prandtl numbers ($Pr = \mu . c_p / k$) of 0.25–2.0. Another study (Henkes and Le Quéré, 1996) investigated the stability of natural convective airflow in a square enclosure with differentially heated vertical walls and lateral periodic boundary conditions. Contrary to previous assumptions, the authors demonstrated that three-dimensional perturbations are less stable than two-dimensional ones. Furthermore, three-dimensional configurations require a lower critical Rayleigh number for turbulent transition. Kim et al. (2003) performed a comprehensive study on the onset of convection and convective heat transfer in two fluid types: Ostwald-de-Waele and Ellis fluids. They numerically analysed the transient buoyancy-driven convection of a power-law non-Newtonian fluid in a differentially heated vertical enclosure. Recent numerical studies investigate Soret-driven convection in a 9:1 water-isopropanol mixture within heated cubic cavities under varying gravitational levels (Shevtsova et al., 2006). Vertical velocity, temperature, and concentration profiles are analysed over time, correlated with the solute Rayleigh number to identify convective onset. Penot (1982) explored flow instability in an isothermal open cavity with an extended domain at Grashof numbers (*Gr*) exceeding 10^5, focusing on cavity inclination angles. The findings highlighted that hydrodynamic instability originates from the cavity's upper opening, while thermal instability arises from *Gr* values linked to side-facing apertures.

A numerical study (Le Quéré , 1990) modelled the transition to unstable natural convection using the two-dimensional Navier-Stokes equations under the Boussinesq approximation. The work focused on a water-filled, differentially heated cavity with a vertical aspect ratio of 10. Results showed that adiabatic walls require a critical Rayleigh number over 30 times higher than conductive walls. However, analysing temperature and velocity fluctuations in both cases showed that boundary layer instability drives unsteady bifurcation. Yang et al. (2002) experimentally investigated Rayleigh-Bénard convection onset in a closed cavity. Their experiment involved two phases: (1) maintaining steady temperatures on the top and bottom plates, and (2) replacing the stationary bottom plate with a moving glass plate. They examined variations in the critical Rayleigh number with cavity depth and explored the effect of shear boundary conditions on the top surface, observed through smoke patterns. Yang and Wang (2019) studied nonlinear heat and mass transfer in a closed cavity with two high-temperature, high-concentration heat sources. They found that increasing the buoyancy ratio reduces the critical Rayleigh number for transitions to periodic or chaotic regimes.

Over the past two decades, extensive theoretical and experimental studies have focused on determining the critical Rayleigh number (*Ra*) for convective onset in enclosures of varying geometries. While some studies suggest conduction dominates heat transfer at *Ra* values ranging from 500 to 2000 (Garcia et al. 2006; Adeyinka, 2005), others report convection initiating at lower *Ra*. Qiao et al. (2008) numerically analysed the transition to chaotic flow in a buoyant plume from a 2D open cavity heated at the base, finding conduction-dominated heat transfer ($Ra \leq 1.4\times10^3$). A 3D numerical simulation of natural convection in a triangular prismatic enclosure (cooled upper surface, heated lower surface) revealed conduction dominance for $Ra < 2\times10^3$, even at *Ra* values spanning $100–1.25\times10^6$ (Cui et al. 2017). Similarly, studies of shallow rectangular cavities (aspect ratio $H/W = 1$, $Pr = 1$) showed conduction dominance for $Ra < 5\times10^3$ (Inaba et al. 1981). In contrast, Vikhansky (2010) investigated natural convection onset in rectangular enclosures filled with Bingham fluids. For $Ra = 200$ ($Pr = 1$) and $Ra = 10^3$ ($Pr = 7$), convection began when the Yield number (*Y*) fell below a critical threshold (Y_{cr}). Once initiated, convection persisted even if *Y* increased, with the Nusselt number stabilising at its conductive value (Nu = 1). Stability analyses of porous cavities, Alves (2002) found conduction dominance ($Nu_{av} = 1$) at $Ra = 50$, transitioning to convection at $Ra = 55$. Flow structures evolved from a single-roll cell ($Ra = 50–200$) to a three-roll system at $Ra = 300$. Mahmud and Andrew (2007) studied entropy generation in

wavy enclosures with microstructures, observing negligible convection at $Ra < 10$ (Nu ≈ 1), regardless of aspect ratio or wall geometry. Natural convection in a cavity with nonuniform wall heating is studied by Turkyilmazoglu (2022) and Alsoy-Akgün (2025). The results showed that the cavity remained filled with a single closed cell at low Rayleigh numbers. Bawazeer and Alsoufi (2025) demonstrated that the onset of natural convection is illustrated by fluid motion at a very low Rayleigh number (i.e. 10). A synergic technique using fins and /or a fan to enhance heat transfer in a cavity at low Rayleigh number is tested by Alok et al. (2026). They found that the enhancement reaches 114.33% at Ra=1000 compared to the baseline case.

The literature review underscores a significant gap in understanding the dynamic behaviour during the initial stages of convection onset at low Rayleigh numbers (*Ra*). These early phases remain underexplored, with scant representation in existing research. To address this gap, this study investigates early-stage flow dynamics in a square cavity during convective onset. Numerical simulations of natural convection are conducted in a cavity with adiabatic horizontal walls, spanning *Ra* (based on cavity height, *H*) from 20 to 1000. Transition mechanisms to unsteady flow are explored, alongside key parameters such as time-averaged temperature, velocity fields, and global heat transfer (quantified via the Nusselt number).

PROBLEM ORMULATION

The system comprises a closed two-dimensional square cavity of side length *H* (Fig. 1). The left and right walls maintain isothermal temperatures T_h and T_c, respectively, while the upper and lower walls are adiabatic. The working fluid is air with a Prandtl number, $Pr = 0.71$, at a reference temperature of 293 K, assumed incompressible and Newtonian. Fluid properties are constant except for density in the buoyancy term, modelled using the Boussinesq approximation. We neglect viscous losses, heat generation, and radiative heat transfer. At low Rayleigh numbers, viscous dissipation and radiative heat transfer are neglected due to minimal velocity gradients and moderate temperature levels, while internal heat generation is omitted in the absence of active heat sources, as per standard practices in Natural Convection studies, see Bejan (2013), Ostrach (198) and Gebhart (1962).

Since convection is purely natural, buoyancy from the Boussinesq term drives the fluid flow. We include the unsteady term in all governing equations to track temporal flow evolution across all Rayleigh numbers (*Ra*).

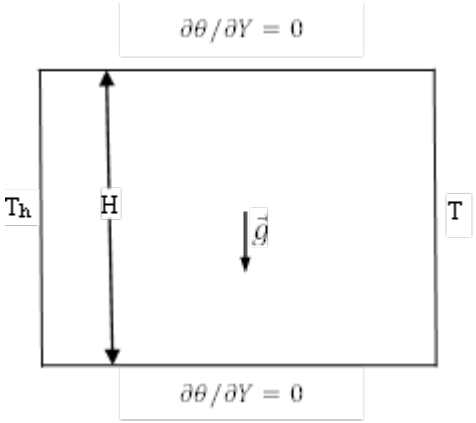

Fig. 1. Schematic diagram of physical model.

The non-dimensional governing equations for mass, momentum, and energy conservation in the unsteady regime are:

$$\frac{\partial U}{\partial X}+\frac{\partial V}{\partial Y}=0 \quad (1)$$

$$\frac{\partial U}{\partial \tau}+U\frac{\partial U}{\partial X}+V\frac{\partial U}{\partial Y}=-\frac{\partial p}{\partial X}+\left(\frac{\partial^2 U}{\partial X^2}+\frac{\partial^2 U}{\partial Y^2}\right) \quad (2)$$

$$\frac{\partial V}{\partial \tau}+U\frac{\partial V}{\partial X}+V\frac{\partial V}{\partial Y}=-\frac{\partial p}{\partial Y}+\left(\frac{\partial^2 V}{\partial X^2}+\frac{\partial^2 V}{\partial Y^2}\right)+\frac{Ra}{Pr}\theta \quad (3)$$

$$\frac{\partial \theta}{\partial \tau}+U\frac{\partial \theta}{\partial X}+V\frac{\partial \theta}{\partial Y}=\frac{1}{Pr}\left(\frac{\partial^2 \theta}{\partial X^2}+\frac{\partial^2 \theta}{\partial Y^2}\right) \quad (4)$$

The flow behaviour is primarily controlled by two dimensionless parameters: the Rayleigh number (Ra) and the Prandtl number (Pr). These parameters are defined as:

$$Ra=\frac{g.\beta.(T_h-T_c).H^3}{\nu^2}.Pr \quad (5)$$

$$Pr=\frac{\mu.Cp}{k} \quad (6)$$

The non-dimensional variables are:

$$X=\frac{x}{H},\ Y=\frac{y}{H},\ \tau=\frac{t}{(H^2/\nu)} \quad (7)$$

$$U=\frac{uH}{\nu},\ V=\frac{\nu H}{\nu} \quad (8)$$

$$\theta=\frac{T-T_c}{T_h-T_c} \quad (9)$$

where *u* and *v* are the horizontal and vertical velocity components, *x* and *y* are Cartesian coordinates, *v* is the kinematic viscosity, *H* is the cavity side length, *T* is the temperature, *g* is the gravitational acceleration, and subscripts *h* and *c* denote the hot and cold walls, respectively.

The thermal and dynamic boundary conditions considered at the walls are as follows:

Left wall *(X=0, 0≤ Y ≤1): U=V=0,* $\theta=1$;

Right wall *(X=1, 0≤ Y ≤1): U=V=0,* $\theta=0$;

Horizontal walls *(0≤ X ≤1 Y=0* and *Y=1): U=V=0,* $\frac{\partial \theta}{\partial Y}=0$.

Table 1: Grid independence test for Ra=10^3

Grid sizes	100×100	150×150	230×230	280×280
Nu_{Av} (at X=0)	1.247	1.172	1.125	1.124

All computations are conducted using the open-source OpenFOAM® CFD code to solve the governing partial differential equations via the buoyantBoussinesqPimpleFoam solver. The PIMPLE algorithm is essentially a hybrid approach, integrating the Semi-Implicit Method for Pressure-Linked Equations (SIMPLE) (Patankar, 1980) with the Pressure Implicit with Splitting Operators (PISO) algorithm (Issa, 1986). Convection terms were discretised with a second-order upwind scheme, and diffusion terms with a second-order central difference scheme. Time-dependent terms were solved using a second-order implicit method, with adaptive time steps constrained by a CFL condition (CFL < 1). Simulations employ a transient solver until reaching steady-state conditions, with time steps adjusted according to the Rayleigh number (Ra).

GRID INDEPENDENCE AND VALIDATION

A grid independence study ensured accuracy while minimising computational costs (e.g., memory and runtime). Simulations employed four mesh resolutions: 100×100, 150×150, 230×230, and 280×280, at $Ra = 10^3$. The Nusselt number difference between the two finest meshes was less than 1% (Table 1), prompting the selection of the 230×230 grid for all subsequent simulations.

The model was validated against De Vahl Davis's (1983) benchmark for a square cavity with isothermal vertical walls (T_h, T_c). As shown in Table 2, differences in Nu remain below 0.6% at $Ra = 10^3$ and 0.3% at 10^4, while results for $Ra = 10^6$ align perfectly with the benchmark.

Table 2: Comparison of present values of average Nu with benchmark solutions.

Ra	Present work	Benchmark (De Vahl Davis, 1983)
	Nu_{Av} (at X=0)	
10^3	1.124	1.117
10^4	2.245	2.238
10^5	4.524	4.509

RESULTS AND DISCUSSION

Flow characteristics evolution:

This study examines the early onset of natural convection at low Rayleigh numbers (Ra), which arise under weak temperature gradients in a square cavity with conductive boundaries. Convective onset is tracked via the temporal evolution of velocity components at fixed monitoring points, streamline analysis across the cavity, and evaluating the Nusselt number (Nu), quantifying the convective-to-conductive heat transfer ratio. Convection is considered dominant once $Nu > 1$, but pre-convective fluid motion begins earlier, even at low velocities. Notably, even gradual pre-convective motion may be undesirable in some applications. The work also investigates temporal flow and thermal evolution during early-stage convection under longitudinal temperature gradients.

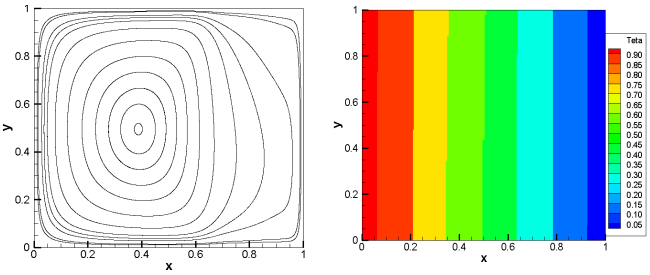

Fig. 2: Streamlines (left) and isotherms (right) at Ra=20

From the initial stages of convective onset to the establishment of quasi-steady or unsteady flow, the flow and thermal characteristics in the cavity evolve dynamically before stabilising or transitioning to instability. Temporal changes in the V-velocity component at sensitive monitoring points reveal flow bifurcations. To observe the flow bifurcation, we established three monitoring points: the first located within the ascending fluid zone (point 1: X=0.25, Y=0.5), and the other two placed in the descending area, close to the boundary separating the primary circulation cell (point 2: X=0.5, Y=0.5) and (point 3: X=0.6, Y=0.5). Thus, the velocity time history can identify sudden velocity increases at the separation point and highlight rapid fluctuations in the flow. This configuration enabled precise monitoring of flow behaviour throughout the distinct regions. Depending on the Rayleigh number (Ra), the final flow structure varies from single- to multi-cellular configurations.

For low Ra values ($Ra < 30$), flow development is extremely slow. When a temperature gradient is applied to the vertical walls from an initial state of rest, fluid motion initiates gradually, forming a single large cell that occupies the cavity without intermediate states. Streamlines and isotherms for $Ra = 20$ (Fig. 2) illustrate this behaviour. Near the heated wall, the streamlines run parallel the wall but curve circularly toward the central cell near the adiabatic boundaries. Adjacent to the cold wall, the

streamlines transition from parallel to quasi-parabolic shapes before merging into the central cell. This asymmetry arises from the higher velocity of the upward buoyant flow compared to the downward flow, indicating slower cooling rates relative to heating. At low Rayleigh numbers, isotherms align quasi-vertically with the temperature gradient, highlighting the weak influence of convection. For Rayleigh numbers in the range $30 < Ra < 200$, flow and thermal patterns differ significantly from those at Ra<30. Figure 3 illustrates the temporal evolution of streamlines and isotherms for *Ra*=100, showing the transition from stagnant fluid to a stable convective state (Lei et al., 2008; Cui et al. 2015). This process involves dynamic stages of flow detachment, reattachment, and separation, leading to the formation of transient cells with varying shapes and sizes.

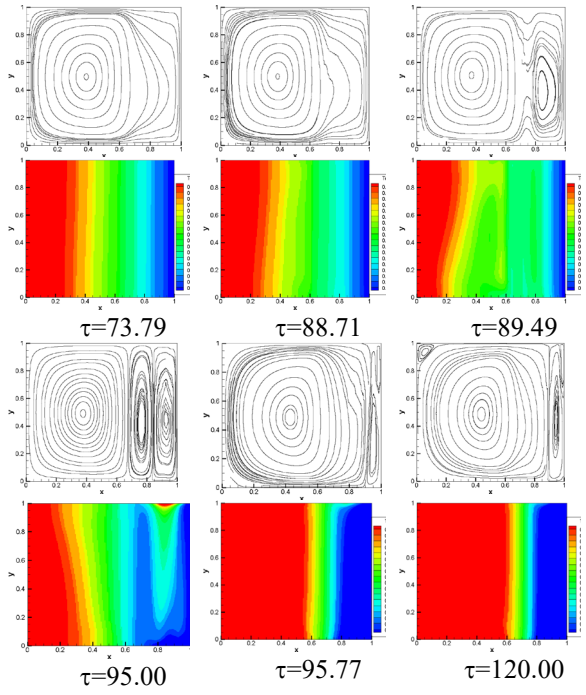

Fig. 3: Streamlines (top) and isotherms at different (bottom) times for Ra=100.

At $Ra = 100$, the flow feature evolves as follows:

-Early stages ($\tau < 73.79$): A single cell occupies the cavity as heating initiates weak fluid motion.

-Intermediate phase: Horizontal flow near the upper adiabatic wall cools, increasing density and triggering downward motion. Shear effects distort streamlines, forming two small vortices.

-Late stages: These vortices, lacking independent momentum, merge back into the primary cell as they approach the cold wall.

-By $\tau = 98.13$ (Fig. 5), a small vortex forms at the hot wall's upper corner, though its upward growth is suppressed by downward buoyancy (Xu et al., 2019).

Heat transfer remains diffusion-dominated, evidenced by quasi-vertical isotherms. However, cooling-induced density gradients drive localized convection.

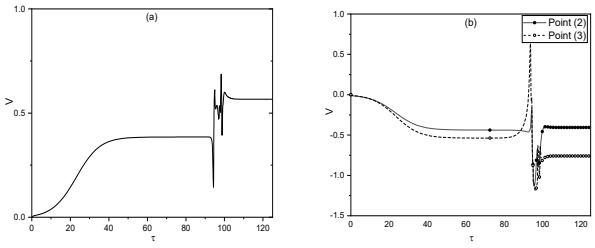

Fig. 4: The V velocity component history at (a): point 1 (X=0.250, Y=0.50); (b): point 2 (X=0.5, Y=0.50), point 3 (X=0.6, Y=0.5) for Ra=100.

To track transitions, we analyse the temporal evolution of velocity components at the three monitoring points:

At $Ra = 100$, the velocity profiles show (Fig. 4):

- Point 1: Due to buoyancy forces, the vertical velocity (V-velocity) increases from zero, where the fluid was initially at rest, up to an intermediate level (approximately 0.39) prior to separation (Fig. 4.a). This effect subsequently spreads throughout the cavity, exhibiting delays in both time and amplitude. Velocity fluctuations are observed during the separation, after which the velocity gradually increases until reaching a steady-state flow velocity of approximately 0.57 after about 100 dimensional time units.

- At points (2) and (3) —both in the descending flow region—the velocity starts at zero (rest) and levels out at a steady intermediate value after roughly 50 time units (Fig. 4.b). After that, the behavior mirrors what we see at point (1): as the circulation cell separates, the velocity fluctuates before eventually stabilizing around $\tau = 100$. One interesting detail: the velocity at point (2) is higher than at point (3). This makes sense because point (3) is farther from the center of the cell.

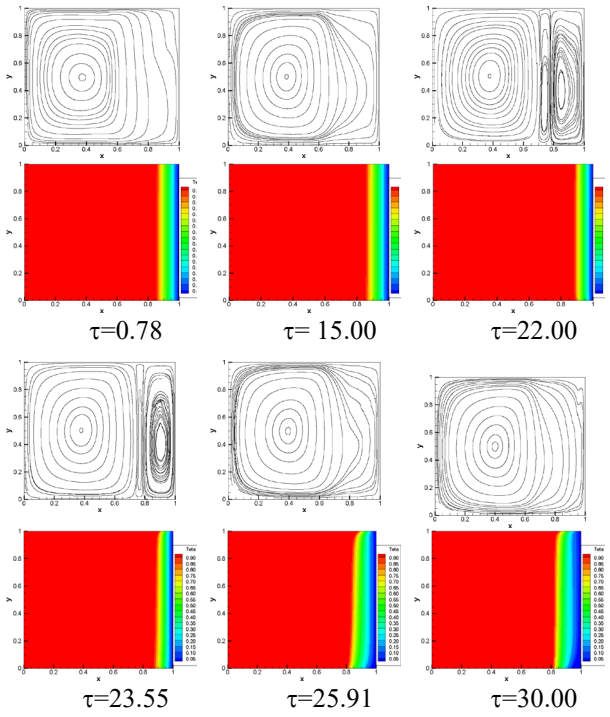

Fig. 5: Streamlines (top) and isotherms at different (bottom) times for Ra=500.

-When the Rayleigh number climbs to *Ra* >100, the flow evolution follows a similar pattern—but with some important differences in shape and timing. One key change is that the small cell near the cold wall shrinks as *Ra* increases and completely disappears by *Ra* = 500 (Fig. 5). The same goes for the upper-corner vortex near the hot wall. This change is accompanied by the loss of the upper-corner vortex near the hot wall. Together, these structural transformations reflect the flow sensitivity, complex dynamics and interactions that emerge as the Rayleigh.

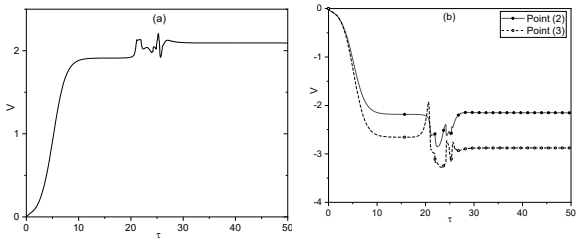

Fig. 6: The V velocity component history at (a): point 1 (X=0.25, Y=0.50); (b): point 2 (X=0.5, Y=0.50) and point 3 (X=0.6, Y0.5) for Ra= 500.

At *Ra* = 250, the main cell separates at $\tau \approx$ 40.82, while at *Ra* = 500, the separation starts earlier ($\tau \approx$ 19.20). Steady-state flow stabilises by $\tau \approx$ 47.57 (*Ra* = 250) and $\tau \approx$ 30.62 (*Ra* = 500). Temporal trends are evident in the *V*-velocity history at monitoring points is showed Fig. 6. As can be seen, increasing *Ra* from 100 to 500 reduces the first perturbation time by >75%, with an additional ~50% reduction at *Ra* = 1000.

These results underscore *Ra* profound influence on flow dynamics, accelerating transitions and altering velocity profiles. Higher *Ra* values correlate with faster stabilisation, likely due to stronger buoyancy-driven convection.

At steady state, the *V*-velocity at Point 1 exceeds pre-perturbation values by ~10%, while Point 2 retains its pre-separation velocity. Specifically, an increase of approximately 10% velocity is observed at point 1, whilst point 3 exhibits a decline of 9% in intensity, and point 2 displays while remaining constant at point 2.

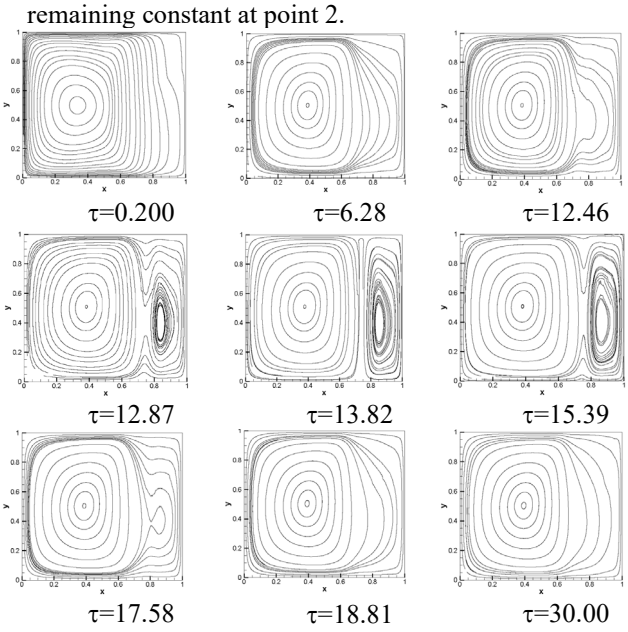

Fig. 7: Streamlines at different times for Ra=1000.

At Ra=1000, the flow feature stars with a large cell left center shifted occupies the whole cavity, as can be seen from the flow feature evolution (Fig. 7). Around τ=12.5, the circulation cell begins to deform near the upper right corner, marking the onset of a structural transition. In response to the disturbance, the fluid takes a shorter path, which induces the formation of a secondary vortex near the cold wall, entrained by the motion of the main circulation cell. Once the secondary cell has formed, the fluid from the main circulation cell is gradually carried away over time, causing it to vanish completely around τ=18. It should be noted that the final steady state is similar to that obtained by Bawazeer and Alsoufi (2025) at comparable Rayleigh number values.

The V-velocity evolution (Fig. 8) shows how the vertical velocity component changes over time at the three distinct sites, (0.25, 0.5), (0.5, 0.5) and (0.6, 0.5). Due to the flow being either upwards (at the first point) or downwards (at the second point and the third points), the horizontal velocity component at these points progress relatively faster than for

Ra=500 where it need only 6-time units to reach the first steady state step. During the τ about 12-16, the velocity component undergoes quasi-random fluctuations, primarily induced by the separation of cells as observed in the streamline contours. A time offset is noticeable in the onset of fluctuations between the velocity evolution at point (0.25, 0.5) compared to that at point (0.6, 0.5). This time delay corresponds to the time required for the transfer of momentum by diffusion and convection. Beyond this point, the flow stabilizes, and the velocity at the monitored locations remains effectively constant. It is worth noting that following the disturbance, the velocity exhibits a variation of less than 5%.

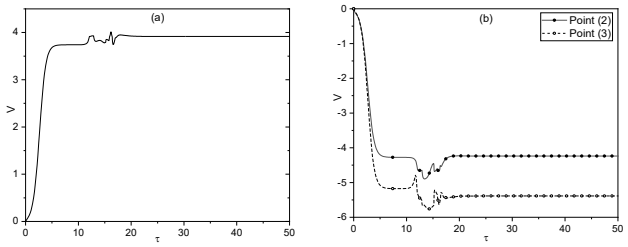

Fig. 8: The V velocity component history at: (a) point (X=0.25, Y=0.50); (b) point 2 (X=0.50, Y=0.50) and point 3 (X=0.6, Y=0.5) For Ra=1000.

Heat Transfer:

Convection is typically defined as occurring when the Nusselt number exceeds unity by a significant margin unity. However, buoyancy-driven flow may initiate much earlier, often during initial stages of the process. At sufficiently low Rayleigh numbers, specifically when Ra falls below an undetermined threshold (not quantified in this study), the fluid exhibits quasi-stagnant behaviour, and the contribution of convective heat transfer becomes negligible. Within this Ra regime, the maximum velocity magnitude does not remain below 3 mm/h.

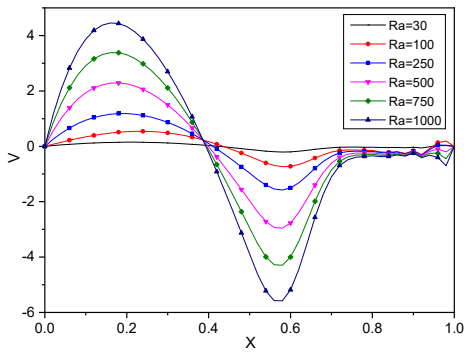

Fig. 9: V Velocity profile along the mid-line cavity at different values of Ra.

The augmentation in heat transfer that is associated with fluid motion becomes perceptible only when the fluid velocity exceeds a critical threshold. In the context of natural convection, this velocity is directly governed by the temperature gradient imposed on the cavity walls, and the Rayleigh number serves as the dimensionless parameter that characterises this relationship. In essence, the Rayleigh number determines the point at which the fluid's motion becomes significant enough to substantially influence heat transfer rates in natural convection scenarios. As depicted in Figure 9, when $Ra < 250$, the maximum upward (dimensionless) velocity near the heated wall does not exceed unity. Consequently, at such low *Ra* values, the convective heat transfer is minimal, although it may promote fluid mixing and induce undesirable outcomes in certain applications. The corresponding Nusselt number, plotted against the Rayleigh number, is shown in Figure 10.

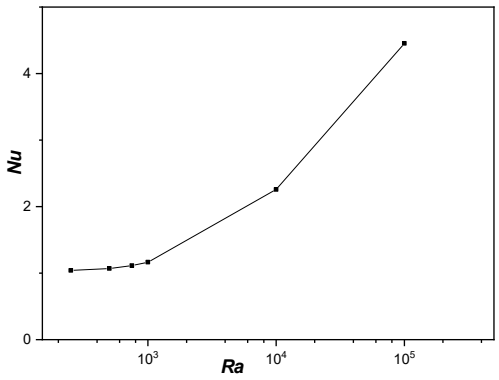

Fig.10: Variation of Nusselt number with Ra.

The Nusselt number exceeds unity when Ra reaches approximately 250. At this *Ra* value, fluid particle motion is too weak to convect energy effectively. The heat convected by fluid motion becomes significant compared to conduction only when the dimensionless velocity exceeds the unity. For *Ra* values between 250 and 800, the energy carried by convection remains below that transported by conduction. However, at $Ra = 1000$, the maximum velocity reaches four times the reference velocity (used for dimensionless scaling), leading to convective heat transfer surpassing conductive heat transfer by a factor of two.

These Nusselt number values obtained at low Rayleigh numbers are comparable to those presented by Bawazeer and Alsoufi (Alsoy-Akgün, 2025) at Ra<1000.

1. CONCLUSION

This computational investigation elucidates the early stages of natural convection within a square cavity. By systematically analysing flow patterns, velocity components, and heat transfer characteristics across Rayleigh numbers (*Ra*) spanning quiescent to convective regimes, three key findings emerge:

- Flow initiation at low *Ra* ($Ra < 250$) is characterised by quasi-steady single-cell

circulation and quasi-vertical isotherms, with heat transfer dominated by conduction (<5% convective contribution).

- At moderate Ra ($250 \leq Ra \leq 800$), dynamic flow transitions occur, including boundary layer detachment, vortex formation, and a progressive reduction in flow stabilisation time (e.g., steady-state attainment accelerates by ~40% at Ra = 500).

- At $Ra = 1000$, convection dominates, with velocity magnitudes quadrupling relative to the reference scale and convective heat transfer surpassing conduction by a factor of two.

These results underscore Ra as the critical parameter governing flow morphology and thermal transport efficiency. The transition from diffusion-dominated to convection-driven behaviour has direct implications for thermal management systems, particularly in microscale electronics or latent heat storage, where early-stage convective dynamics dictate performance.

This study establishes a foundation for future work exploring three-dimensional geometries, transient boundary conditions, or multicomponent fluids to refine predictive models for industrial applications.

REFERENCES

Adeyinka, O. B. and Naterer, G. F. "Particle Image Velocimetry Based Measurement of Entropy Production With Free Convection Heat Transfer," *Transactions of the ASME*., Vol. 127, no. 6, pp. 614–623 (2005). DOI: 10.1115/1.1863272

Akbarzadeh, M., Rashidi, S., Karimi, N. and Ellahi, R. "Convection of heat and thermodynamic irreversibilities in two-phase, turbulent nanofluid flows in solar heaters by corrugated absorber plates," *Adv. Powder* Technol, Vol. 29, no. 9, pp. 2243–2254 (2018). DOI:10.1016/j.apt.2018.06.009

Alam, T. and Kim, M. H. "A comprehensive review on single phase heat transfer enhancement techniques in heat exchanger applications," Renew. Sustain. Energy Rev., Vol. 81, Part 1, pp. 813–839 (2018). DOI: 10.1016/j.rser.2017.08.060

Alok, U., Rahaman, M. and Devanuri, J. K. "Synergistic effects of passive and active heat transfer enhancement strategies in a confined domain," *Int. J. Heat Fluid Flow,* vol. 117, part A, *paper* 110060 (2026). DOI: 10.1016/j.ijheatfluidflow.2025.110060

Alsoy-Akgün, N. "Natural convection resulting from exponentially varying wall heating in a square enclosure," *Comput. Math. Appl.,* Vol. 197, pp. 235-258 (2025). DOI: 10.1016/j.camwa.2025.08.024

Alves, L. S. de B., Cotta, R. M. and Pontes, J. "Stability analysis of natural convection in porous cavities through integral transforms," *Int. J. Heat Mass Transf.,* Vol. 45, no. 6, pp. 1185–1195 (2002). DOI: 10.1016/S0017-9310(01)00231-9

Batchelor, G. K. "Heat transfer by free convection across a closed cavity between vertical boundaries at different temperatures," *Q. Appl. Math.,* Vol. XII, no. 3, pp. 209–233 (1954). DOI: 10.1090/QAM/64563

Bawazeer, S. A. and Alsoufi, M. S. "Natural convection in a square Cavity: Effects of Rayleigh and Prandtl numbers on heat transfer and flow patterns," Case Stud. Therm. Eng., Vol. 73, *paper* 106680 (2025). DOI: 10.1016/j.csite.2025.106680

Bejan, A. *Convection Heat Transfer*, 4th Edition, John Wiley & Sons (2013).

Bejan, A. *Heat Transfe*r, John Wiley and Sons, Inc. New York (1993).

Cui, H., Xu, F. and Saha, S. C. "Transition to unsteady natural convection flow in a prismatic enclosure of triangular section," *Int. J. Therm. Sci.,* Vol. 111, pp. 330–339 (2017). DOI: 10.1016/j.ijthermalsci.2016.09.008

Cui, H., Xu, F. and Saha, S. C. "A three-dimensional simulation of transient natural convection in a triangular cavity," *Int. J. Heat Mass Transf.,* Vol. 85, pp. 1012–1022 (2015). DOI: 10.1016/j.ijheatmasstransfer.2015.02.046

De Vahl Davis, G. "Natural convection of air in a square cavity: a benchmark numerical solution," *Int. J. Numer. Methods Fluids.,* Vol. 3, pp. 249–264 (1983). DOI: 10.1002/fld.1650030305

Garcia, O. E., Bian, N. H., Naulin, V., Nielsen, A. H. and Rasmussen, J. J. "Two-dimensional convection and interchange motions in fluids and magnetized plasmas," Physica Scripta., Vol. T122, pp. 104–124 (2006). DOI: 10.1088/0031-8949/2006/T122/014

Gebhart, B. "Effects of viscous dissipation in natural convection," *J. Fluid Mech.,* Vol. 14, Issue 2, pp. 225-232 (1962). DOI: 10.1017/S0022112062001196

Henkes, R. A. W. M. and Le Quéré, P. "Three-dimensional transition of natural convection flows," *J. Fluid Mech.,* Vol. 319, pp. 281–303 (1996). DOI: 10.1017/S0022112096007343

Inaba, H., Seki, N., Fukusako, S. and Kanayama, K. "Natural convective heat transfer in a shallow rectangular cavity with different end temperatures," *Numer. Heat Transf.,* Vol. 4, no. 4, pp. 459-468 (1981). DOI: 10.1080/01495728108961804

Issa, R. I. "Solution of the implicitly discretised fluid flow equations by operator-splitting," *J. Comput. Phys.,* Vol. 62 (1), pp. 40-65 (1986). DOI: 10.1016/0021-9991(86)90099-9

Janssen, R. J. A. and Henkes, R. A. W. M. "Influence of Prandtl number on instability mechanisms and transition in a differentially heated square cavity," *J. Fluid Mech.,* Vol. 290, pp. 319–344 (1995). DOI: 10.1017/S0022112095002539

Khan, A. A., Naeem, S., Ellahi, R., Sait, S. M. and Vafai, K. "Dufour and soret effects on Darcy-Forchheimer flow of second-grade fluid with the variable magnetic field and thermal conductivity," *Int. J. Numer. Methods Heat Fluid Flow,* Vol. 30, no. 9, pp. 4331–4347 (2020). DOI: 10.1108/HFF-11-2019-0837

Kim, G. B., Hyun, J. M. and Kwak, H. S. "Transient buoyant convection of a power-law non Newtonian fluid in an enclosure," *Int. J. Heat Mass Transfer.,* Vol. 46, no. 19, pp. 3605–3617 (2003). DOI: 10.1016/S0017-9310(03)00149-2

Le Quéré, P. "Transition to unsteady natural convection in a tall water-filled cavity," *AIP Physics of Fluid.,* Vol. 2, no. 4, pp. 503-515 (1990). DOI: 10.1063/1.857750

Lei, C., Armfield, S. W. and Patterson, J. C. "Unsteady natural convection in a water-filled isosceles triangular enclosure heated from below," *Int. J. Heat Mass Transf.,* Vol. 51, no. 11-12, pp. 2637–2650 (2008). DOI: 10.1016/j.ijheatmasstransfer.2007.09.001

Li, Y., Yang, M., Li, J. and Wang, Z. "Study on heat and mass transfer and nonlinear characteristics with thermal and solutal source in a cavity," *Front. Heat Mass Transf.,* Vol. 13, pp. 1-8, (2019). DOI: 10.5098/hmt.13.11

Liu, Y., Zhang, S., Huang, H., Suo, Q., Bian, Y. and Zhao, Y. "Enhancing the flow and heat transfer in a convective cavity using symmetrical and adiabatic twin fins," *Int. J. Heat Mass Transf.* Vol. 142, *paper* 118447 (2019). DOI: 10.1016/j.ijheatmasstransfer.2019.118447

Mahmud, S., Fraser, R. A. and Pop, I. "Flow, Thermal, Energy Transfer, and Entropy Generation Characteristics Inside Wavy Enclosures Filled With Microstructures," *J. Heat Transfer.,* Vol. 129, no. 11, pp. 1564–1575 (2007). DOI: 10.1115/1.2759976

Ostrach, S. "Natural Convection in Enclosures," *ASME, J. Heat Transfer.,* Vol. 110, pp. 1175-1190 (1988). DOI: 10.1115/1.3250619

Patankar, S. V. Numerical heat transfer and fluid flow, CRC, New York, USA: Hemisphere (1980).

Penot, F. "Numerical calculation of two-dimensional natural convection in isothermal open cavities," *Numer. Heat Transfer.,* Vol. 5, no. 4, pp. 421-437 (1982). DOI: 10.1080/10407788208913457

Qiao, M., Xu, F. and Suvash, C. S. "Numerical study of the transition to chaos of a buoyant plume from a two-dimensional open cavity heated from below," *Appl. Math. Model.,* Vol. 61, pp. 577–592 (2018). DOI: 10.1016/j.apm.2018.05.013

Serrano-Arellano, J., Xaman, J. and Alvare, G. "Optimum ventilation based on the ventilation effectiveness for temperature and CO2 distribution in ventilated cavities," *Int. J. Heat Mass Transf.,* Vol. 62, pp. 9–21 (2013). DOI: 10.1016/j.ijheatmasstransfer.2013.02.051

Sharma, S. L. and Debbarma, A. "A review on thermal performance and heat transfer augmentation in solar air heater," *Int. J. Sustain. Energy.,* Vol. 41, no. 2, pp. 1973–2019 (2022). DOI: 10.1080/14786451.2022.2125518

Shevtsova, V. M., Melnikov, D. E. and Legros, J. C. "Onset of convection in Soret-driven instability," *Phys. Rev.,* Vol. 73, no. 4 (2006). DOI: 10.1103/PhysRevE.73.047302

Tanny, J. and Tsinober, A. B. "The dynamics and structure of double-diffusive layers in sidewall-heating experiment," *J. Fluid Mech.,* Vol. 196, pp. 135–156 (1988). DOI: 10.1017/S0022112088002642

Turkyilmazoglu, M. "Exponential nonuniform wall heating of a square cavity and natural convection," *Chin. J. Phys.,* Vol. 77, pp. 2122–2135 (2022). DOI: 10.1016/j.cjph.2021.12.021

Vikhansky, A. "On the onset of natural convection of Bingham liquid in rectangular enclosures," J. Non-Newtonian Fluid Mech., Vol. 165, no. 23-24, pp. 1713–1716 (2010). DOI: 10.1016/j.jnnfm.2010.09.003

Xu, D., Hu, Y. and Li, D. "A lattice Boltzmann investigation of two-phase natural convection of Cu-water nanofluid in a square cavity," *Case Stud. Therm. Eng.,* Vol. 13, *paper* 100358 (2019). DOI: 10.1016/j.csite.2018.11.009

NOMENCLATURE

Cp: specific heat of air, J/(kg · K)

K: thermal conductivity, W/m.K

Nu: Nusselt Number

Nu_{av}: average Nusselt number

Pr: Prandtl number

Ra: Rayleigh Number

Ra_{cr}: critical Rayleigh number

T: temperature, K

T_h: hot temperature, K

T_c: cold temperature, K

t: time, s

U, V: dimensionless velocity components

u, v: velocity components in x and y directions, $m.s^{-1}$

X, Y: dimensionless Cartesian coordinates

x, y: dimensional Cartesian coordinates, m

Greek symbols

β: thermal expansion coefficient, K^{-1}

θ: dimensionless temperature

μ: dynamic viscosity of air, $kg/(s \cdot m)$

ν: kinematic viscosity of air, m^2/s

ρ: density of air, kg/m^3

τ: dimensionless time